Divalent Cation Sensitivity of BK Channel Activation Supports the Existence of Three Distinct Binding Sites

Xu-Hui Zeng,[1] Xiao-Ming Xia,[1] and Christopher J. Lingle[1,2]

[1]Department of Anesthesiology and [2]Department of Anatomy and Neurobiology, Washington University School of Medicine, St. Louis, Missouri 63110

ABSTRACT Mutational analyses have suggested that BK channels are regulated by three distinct divalent cation-dependent regulatory mechanisms arising from the cytosolic COOH terminus of the pore-forming α subunit. Two mechanisms account for physiological regulation of BK channels by μM Ca^{2+}. The third may mediate physiological regulation by mM Mg^{2+}. Mutation of five aspartate residues (5D5N) within the so-called Ca^{2+} bowl removes a portion of a higher affinity Ca^{2+} dependence, while mutation of D362A/D367A in the first RCK domain also removes some higher affinity Ca^{2+} dependence. Together, 5D5N and D362A/D367A remove all effects of Ca^{2+} up through 1 mM while E399A removes a portion of low affinity regulation by Ca^{2+}/Mg^{2+}. If each proposed regulatory effect involves a distinct divalent cation binding site, the divalent cation selectivity of the actual site that defines each mechanism might differ. By examination of the ability of various divalent cations to activate currents in constructs with mutationally altered regulatory mechanisms, here we show that each putative regulatory mechanism exhibits a unique sensitivity to divalent cations. Regulation mediated by the Ca^{2+} bowl can be activated by Ca^{2+} and Sr^{2+}, while regulation defined by D362/D367 can be activated by Ca^{2+}, Sr^{2+}, and Cd^{2+}. Mn^{2+}, Co^{2+}, and Ni^{2+} produce little observable effect through the high affinity regulatory mechanisms, while all six divalent cations enhance activation through the low affinity mechanism defined by residue E399. Furthermore, each type of mutation affects kinetic properties of BK channels in distinct ways. The Ca^{2+} bowl mainly accelerates activation of BK channels at low [Ca^{2+}], while the D362/D367-related high affinity site influences both activation and deactivation over the range of 10–300 μM Ca^{2+}. The major kinetic effect of the E399-related low affinity mechanism is to slow deactivation at mM Mg^{2+} or Ca^{2+}. The results support the view that three distinct divalent-cation binding sites mediate regulation of BK channels.

KEY WORDS: BK channels • Ca^{2+} regulatory sites • divalent cations • Slo • activation

INTRODUCTION

The sites and mechanisms by which Ca^{2+} binding results in regulation of Ca^{2+}-activated and voltage-dependent BK type K^+ channels (Barrett et al., 1982; Moczydlowski and Latorre, 1983; Horrigan and Aldrich, 2002; Lingle, 2002; Magleby, 2003) remain incompletely understood. Available evidence suggests that the Ca^{2+} regulatory machinery is contained in the extensive cytosolic COOH terminus of each BK channel α subunit (Schreiber and Salkoff, 1997; Schreiber et al., 1999; Bian et al., 2001; Bao et al., 2002; Shi et al., 2002; Xia et al., 2002, 2004), but that physiological regulation by Ca^{2+} is defined by multiple determinants in the COOH terminus. Specifically, mutational analyses indicate that at least three distinct Ca^{2+} regulatory mechanisms in each α subunit may influence activation of BK channels, two of μM affinity mediating physiological regulation by Ca^{2+} (Schreiber and Salkoff, 1997; Bao et al., 2002; Xia et al., 2002) and one of lower affinity perhaps providing the basis for channel regulation by cytosolic Mg^{2+} (Shi et al., 2002; Xia et al., 2002). However, except perhaps for the so-called Ca^{2+} bowl residues (Schreiber and Salkoff, 1997; Bian et al., 2001; Bao et al., 2004), the extent to which these mutationally defined loci correspond to specific divalent cation binding sites remains unclear. In addition, the extent to which the three distinct regulatory effects are coupled or independent remains unknown.

Explicit structural information about the BK channel COOH terminus remains unavailable. However, the recognition that domains within the BK channel COOH terminus exhibit homology to ligand-binding RCK (regulatory of conductance for K^+) domains of bacterial K^+ channels (Jiang et al., 2001, 2002) provides a substantive guide to evaluating the BK channel cytosolic structure. Specifically, the Ca^{2+}-regulated MthK bacterial K^+ channel exhibits an octameric arrangement of RCK domains, with each RCK domain proposed to contain a Ca^{2+}-binding site (Jiang et al., 2002). Similarly, the COOH terminus of each BK channel α subunit has also been proposed to contain a pair of RCK domains (Jiang et al., 2002; Roosild et al., 2004). Whereas the homology of the first RCK domain in the BK channel α

Correspondence to Chris Lingle: clingle@morpheus.wustl.edu

Abbreviation used in this paper: RCK, regulatory of conductance for K^+.

J. Gen. Physiol. © The Rockefeller University Press • 0022-1295/2005/03/273/14 $8.00
Volume 125 March 2005 273–286
http://www.jgp.org/cgi/doi/10.1085/jgp.200409239

subunit to bacterial RCK domains is fairly well defined, the second BK RCK domain is less clear (Roosild et al., 2004). Yet, the model provided by the MthK channel raises the possibility that two ligand binding sites per BK α subunit may be required to produce the conformational changes required for channel opening.

The mutational analysis, in fact, can be viewed as supporting the idea that there are separate Ca^{2+} regulatory elements at least loosely associated with each of the RCK-containing motifs of each α subunit. One of these elements is the Ca^{2+} bowl, an aspartate-rich region near the COOH terminus (Schreiber and Salkoff, 1997). The fact that Ca^{2+} bowl mutations remove only a portion of Slo1 Ca^{2+} dependence suggested that there must be additional Ca^{2+} regulatory sites. Subsequently, two separate loci in the first RCK domain were shown to disrupt a second component of Slo1 regulation by micromolar Ca^{2+} (Bao et al., 2002; Xia et al., 2002). Residues D362 and D367 were identified by a search for negatively charged residues in the first RCK domain that were shared among all Slo1 homologues, but not found in the Ca^{2+}-independent, pH-regulated Slo3 channel (Xia et al., 2002). The D362A/D367A mutation, in conjunction with mutation of the Ca^{2+} bowl, results in complete abolition of Slo1 regulation up to 1 mM Ca^{2+}. Another mutation, M513I, behaved in a fashion similar to the D362A/D367A mutation (Bao et al., 2002), both mutations removing a similar component of regulation by Ca^{2+}. Thus, these results suggest that distinct Ca^{2+} binding sites, associated with two distinct modules in the COOH terminus of the BK channel α subunit, may account for regulation of Slo1 current by micromolar Ca^{2+}. Finally, a third set of residues, also in the first RCK domain, participates in regulation by mM Ca^{2+} or Mg^{2+} (Shi and Cui, 2001; Xia et al., 2002). While Ca^{2+} overlay assays have supported the idea that the Ca^{2+} bowl may bind divalent cations directly (Bian et al., 2001; Braun and Sy, 2001; Bao et al., 2004), at present there is no information about Ca^{2+} binding to the first RCK domain. Thus, in the absence of such information, it remains possible that the mutations in the first RCK domain do not represent a distinct binding site, but simply disruption of a component of Ca^{2+} regulation initiated by a single Ca^{2+} binding site elsewhere on the protein.

We hypothesize that if each regulatory mechanism involves a distinct divalent cation binding site, each mechanism might exhibit differences in selectivity among different divalent cations. In fact, it has been previously observed that the functional disruption of the calcium bowl does not disrupt BK channel regulation produced by Cd^{2+}, leading to the suggestion that the BK channel may contain additional Ca^{2+} regulatory sites (Schreiber and Salkoff, 1997). A number of other divalent cations, such as Mn^{2+}, Ni^{2+}, and Co^{2+}, are also known to regulate BK activation (Oberhauser et al., 1988), but how their effects relate to known regulatory mechanisms is unknown. We have therefore evaluated the divalent cation sensitivity of each of the three mutationally defined processes contributing to regulation of BK channels. Furthermore, to assess whether the regulatory sites act independently or in concert to regulate BK gating, we also examined the kinetic consequences of mutation of each regulatory site.

Our results show that each mutationally defined regulatory mechanism exhibits a sensitivity to a set of divalent cations distinct from each of the other two regulatory mechanisms. This argues strongly that each regulatory mechanism involves a specific and unique divalent cation binding site located on each α subunit, although it does not establish that the mutated residues contribute to cation coordination. Furthermore, each regulatory site exerts distinct effects on channel kinetic behavior. The results support the idea that there are three distinct divalent cation binding sites that contribute in independent ways to regulation of BK channel activation.

MATERIALS AND METHODS

Generation and Expression of mSlo1 Mutants

The wild-type construct for these studies was mouse Slo1 (mSlo1) (Butler et al., 1993), generously provided by L. Salkoff (Washington University, St. Louis, MO). Numbering used here for mSlo1 residues begins with the second potential initiation site. Construction of mutations was as previously described (Xia et al., 2002). Disruption of Ca^{2+} bowl function was accomplished by neutralization of five consecutive aspartic acid residues in that region (5D5N; mSlo1 residues 897 through 901). Mutations in the first RCK domain disrupted another high affinity Ca^{2+} regulatory effect (D362A/D367A), while a mutation in a second location in the first RCK domain (E399A) disrupted low affinity regulation by Mg^{2+} and Ca^{2+}. We have also confirmed that mutation of E374A, another residue implicated in low affinity Mg^{2+} regulation (Shi et al., 2002), produces effects on regulation by Mg^{2+} identical to those of E399A (not depicted). Simultaneous mutation of both E374A and E399A produced no additional effect beyond that occurring with each mutation of each residue alone.

Methods of expression in *Xenopus* oocytes were as previously described (Zeng et al., 2001, 2003). SP6 RNA polymerase was used to synthesize cRNA for oocyte injection after DNA was linearized with M1uI. 10–50 nl of cRNA (10–20 ng/μl) was injected into stage IV *Xenopus* oocytes harvested 1 d before. Oocytes were used 2–7 d after injection of cRNA.

Electrophysiological Recordings

Channel currents were recorded from inside-out patches (Hamill et al., 1981) using Clampex (Axon Instruments), as performed routinely in our laboratory (Lingle et al., 2001; Zeng et al., 2003). During electrophysiological recordings, oocytes were maintained in ND96 bath solution (96 mM NaCl, 2.0 mM KCl, 1.8 mM $CaCl_2$, 1.0 mM $MgCl_2$, 5.0 mM HEPES, pH 7.5). The pipette extracellular solution was 140 mM potassium methanesulfonate, 20 mM KOH, 10 mM HEPES, 2 mM $MgCl_2$. Cd^{2+}, Mn^{2+}, Co^{2+}, and Ni^{2+} solutions bathing the cytoplasmic face of the patch membrane

contained 155 mM KF and 10 mM HEPES. Such solutions were typically prepared by adding aliquots of metal-chloride solutions to the KF solution. As noted previously (Oberhauser et al., 1988), because of the lack of solubility of CaF_2, F^- effectively removes free Ca^{2+} from such solutions such that the effective free Ca^{2+} concentrations can be considered <20 nM. In contrast, Cd^{2+}, Mn^{2+}, Co^{2+}, and Ni^{2+} remain soluble. Since Sr^{2+} is insoluble in the presence of F^-, Sr^{2+} solutions were made with 140 mM potassium methanesulfonate, 20 mM KOH, 10 mM HEPES, and buffered with 10 mM EGTA. Appropriate additions of Sr^{2+} were determined with EQCALWIN (Biosoft). Assuming a contaminant Ca^{2+} concentration of 15 μM, free Ca^{2+} in the 2, 5, 10, and 20 mM Sr^{2+} solutions should be ~106, 54, 28, and 11 nM, respectively. None of the effects described here for mM Sr^{2+} are attributable to Ca^{2+} at these concentrations. The pH values of all these solutions were adjusted to 7.0 with methanesulfonic acid or KOH, as required. The methods of calibration and preparation of Ca^{2+} and Mg^{2+} solutions have been described (Zeng et al., 2001). Concentrations of Mn^{2+} >5 mM were not employed because of the formation of precipitates in the MnF solutions. Cd^{2+} concentrations of 1 mM and higher produced essentially irreversible effects on Slo1 currents, perhaps reflecting essentially irreversible binding of Cd^{2+} to particular cytosolic cysteine residues in the cytosolic face of the Slo1 α subunit.

Excised inside-out patches were locally perfused with solutions flowing from a blunt perfusion pipette with an ~150–200-μm tip (Herrington et al., 1995; Solaro et al., 1997). The shank of the perfusion pipette was packed with seven PE10 tubes that were connected to reservoirs containing cytosolic solutions of specific divalent cation composition. Solution flow was permitted from only a single PE10 line at any time, and was activated either by a hand-controlled valve or a computer-controlled solenoid valve. Additional upstream valves allowed a given patch to be tested with up to 10 different solutions. A complete concentration change between a pair of solutions was generally complete at the cytoplasmic face of the patch within several hundred milliseconds.

Current values were measured using ClampFit (Axon Instruments) and converted to conductance. Conductance–voltage (G–V) curves were generated from tail currents following standard procedures (Zeng et al., 2001). Families of G–V curves represent averages from a set of patches at specific divalent cation concentrations. For each patch, G–V curves were fit with the following:

$$G(V) = G_{max}/(1 + \exp^{-(V-V_h)/k}) \quad (1)$$

to provide estimates of V_h, the voltage of half activation, and k, the slope factor describing the voltage dependence of the closed–open equilibrium. For comparison of the magnitude of V_h shifts, ΔV_h values were obtained by subtracting the V_h in the absence of specific divalent ions. Activation and deactivation time constants were obtained by fitting the original current traces by exponential functions. In all cases, error bars show SEM.

Experiments were done at room temperature (21–24°C). 1 N KOH solutions for preparation of physiological solutions was obtained from Fisher Scientific. KF, $MnCl_2$, and $NiCl_2$ were obtained from Alfa-Aesar. All other salts and chemicals were obtained from Sigma-Aldrich.

RESULTS

The results in this paper address two topics. First, the relative divalent cation selectivity of each of the mutationally defined divalent cation regulatory mechanisms is addressed. Second, the impact of each of the mutationally defined regulatory mechanisms on activation and deactivation time course is examined.

Cd^{2+} Activates BK Channels by Acting on the D362/D367 Site but not the Ca^{2+} Bowl

BK currents exhibit a characteristic shift in activation with elevations in cytosolic $[Ca^{2+}]_i$ (Cox et al., 1997). Typically, the voltage of half activation (V_h) obtained from conductance–voltage (G–V) curves shifts to more negative potentials as Ca^{2+} is elevated (Xia et al., 2002). Here, we compare the V_h shifts caused by specific divalent cations for wild-type mSlo1 BK channels and mSlo1 mutants with selective disruption of each of three putative regulatory mechanisms. The ability of mutation of a specific regulatory mechanism to alter the V_h shift produced by a given divalent cation can be taken as evidence for interaction between this cation and the binding site that mediates the regulatory effect. It does not prove that the mutated residues participate in binding site.

It has been previously reported that 60 μM Cd^{2+} activates BK currents, producing a negative V_h shift (Schreiber and Salkoff, 1997). This effect was not altered by mutation of residues in the Ca^{2+} bowl, leading to the proposal that there was a second divalent cation regulatory site (Schreiber and Salkoff, 1997). We therefore examined whether Cd^{2+} selectively activates BK channels through either of the other putative divalent cation regulatory sites.

Representative currents recorded from wild-type mSlo1, D362A/D367A, and 5D5N over a range of $[Cd^{2+}]$ up to 300 μM are shown in Fig. 1 (A–C). At $[Cd^{2+}]$ >300 μM, both steady-state current and tail current amplitudes are largely blocked and the recovery is very slow. The blocking effect of Cd^{2+} on 5D5N seems weaker than that on mSlo1, although Cd^{2+} produces similar V_h shifts for both.

For mSlo1 and 5D5N, as $[Cd^{2+}]$ is increased over the range of 0 through 300 μM, current activation is shifted to more negative activation potentials. In contrast, this is not the case for D362A/D367A. For each construct, G–V curves at different $[Cd^{2+}]$ were obtained from tail currents and fit with a Boltzmann function (Eq. 1) to obtain an estimate of V_h. Within each patch, conductance estimates were normalized to the maximal conductance observed at 30 μM Cd^{2+}. The relative V_h shift (ΔV_h), obtained by subtracting the V_h value at 0 Cd^{2+} from that at given $[Cd^{2+}]$, was used as a relative indication of the ability of Cd^{2+} to enhance activation.

In wild-type mSlo1 channels, Cd^{2+} shifts G–V curves leftward (Fig. 1 D) and produces negative V_h shifts (Fig. 1 G). In contrast, the ability of Cd^{2+} to activate BK channels is largely abolished in D362A/D367A relative to mSlo1, especially when $[Cd^{2+}]$ is 100 μM or below

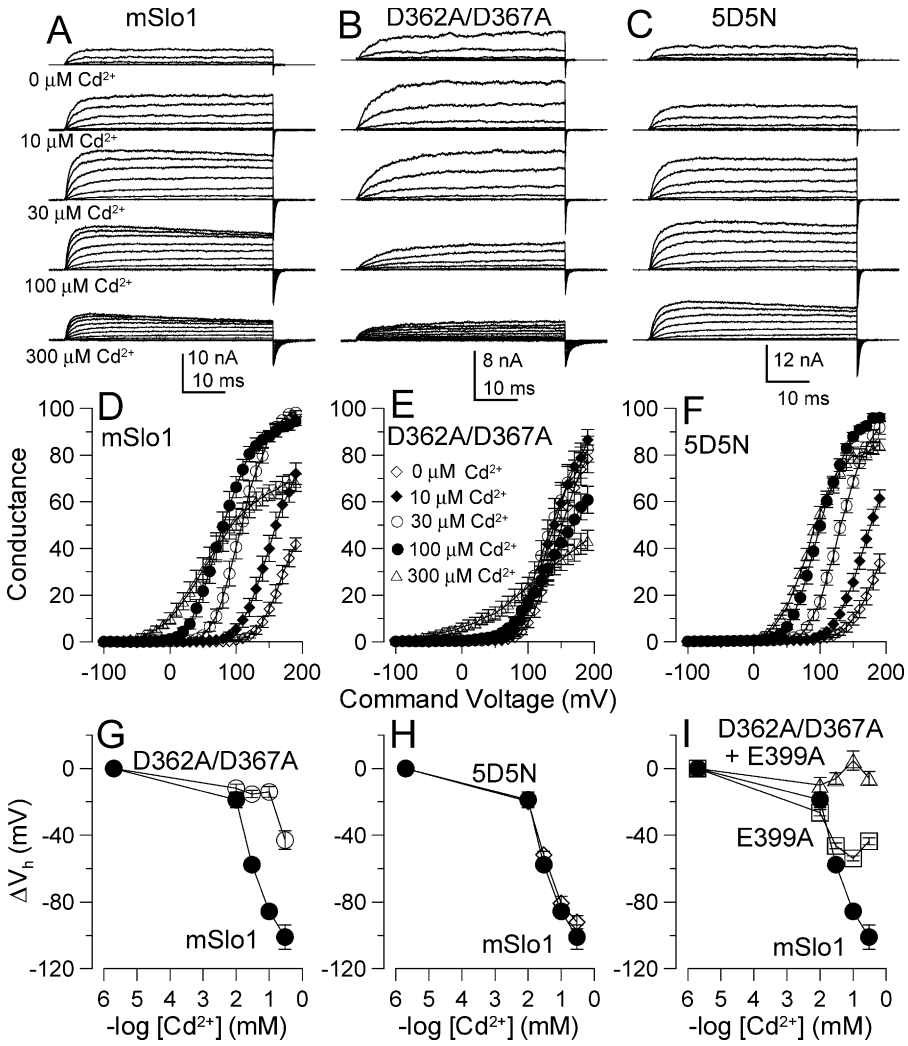

FIGURE 1. Cd^{2+} confers high affinity regulatory effects only through the D362/D367 site. (A–C) Traces show currents from inside-out patches for Slo1 and indicated mutants with cytosolic $[Cd^{2+}]_i$ as shown in A. Voltage steps were from −80 mV through to +160 mV in 20-mV increments following 40 ms at −180 mV, with tail currents at −120 mV. (D-F) G–V curves were generated over $[Cd^{2+}]_i$ from 0 to 300 μM for Slo1 ($n = 6$), D362A/D367A ($n = 7$) and 5D5N ($n = 6$). Open diamonds, 0 μM; filled diamonds, 10 μM; open circles, 30 μM; filled circles, 100 μM; open triangles, 300 μM. Current amplitude is markedly reduced when $[Cd^{2+}]_i$ is >300 μM (not depicted). (G) Activation ΔV_h is plotted versus $[Cd^{2+}]_i$ for wild-type Slo1 ($n = 6$) and for the construct with the D362A/D367A mutation ($n = 7$). (H) ΔV_h is plotted versus $[Cd^{2+}]$ for Slo1 versus 5D5N ($n = 6$). (I) ΔV_h is plotted versus $[Cd^{2+}]$ for Slo1 versus E399A ($n = 7$) and the combined mutation of D362A/D367A + E399A ($n = 8$).

(Fig. 1, E and G). On the other hand, the ability of $[Cd^{2+}]$ to cause current activation is well preserved in 5D5N (Fig. 1, F and H), consistent with previous observations (Schreiber and Salkoff, 1997). Up through 100 μM, Cd^{2+} shows little effect on the voltage dependence of channel gating. However, a more shallow G–V curve is observed at 300 μM Cd^{2+} for both mSlo1 (Fig. 1 D) and D362A/D367A (Fig. 1 E), probably arising in part from the voltage dependence of the mechanism of Cd^{2+} block.

We next examined whether the E399 low affinity site might contribute to the additional V_h shift observed with 300 μM Cd^{2+} in D362A/D367A (Fig. 1 G). For the E399A channel, Cd^{2+} up through 30 μM had effects similar to its effects on wild-type mSlo1. However, V_h shifts at 100 and 300 μM $[Cd^{2+}]$ are largely reduced in the E399A channel compared with results obtained from mSlo1 (Fig. 1 I). Furthermore, for the double mutant, D362A/D367A+E399A, the ability of Cd^{2+} to shift current activation is essentially abolished over the entire test concentration range (Fig. 1 I). The apparently additive effects of D362A/D367A and E399A suggest that these two sites act independently in regards to the ability of Cd^{2+} to regulate BK channels.

In conclusion, it is the regulatory mechanism defined by the D362/D367 site, and not that defined by the Ca^{2+} bowl, which mediates activation of BK channels by lower concentrations of Cd^{2+}. At higher concentrations, Cd^{2+} also can enhance channel activation through the low affinity site defined by E399.

Mn^{2+} Enhances Activation of BK Channels through the E399 Low Affinity Site

Mn^{2+} has been shown to activate muscle membrane BK channels expressed in bilayers (Oberhauser et al., 1988). We therefore tested whether the ability of Mn^{2+} to modulate BK channels might be selectively associated with any of the three putative regulatory sites. Fig. 2 (A–C) shows currents activated in the presence of 0 through 5 mM Mn^{2+} for mSlo1, E399A, and the triple mutation (5D5N+D362A/D367A+E399A). For mSlo1, Mn^{2+} causes a leftward shift in the G–V curves with no

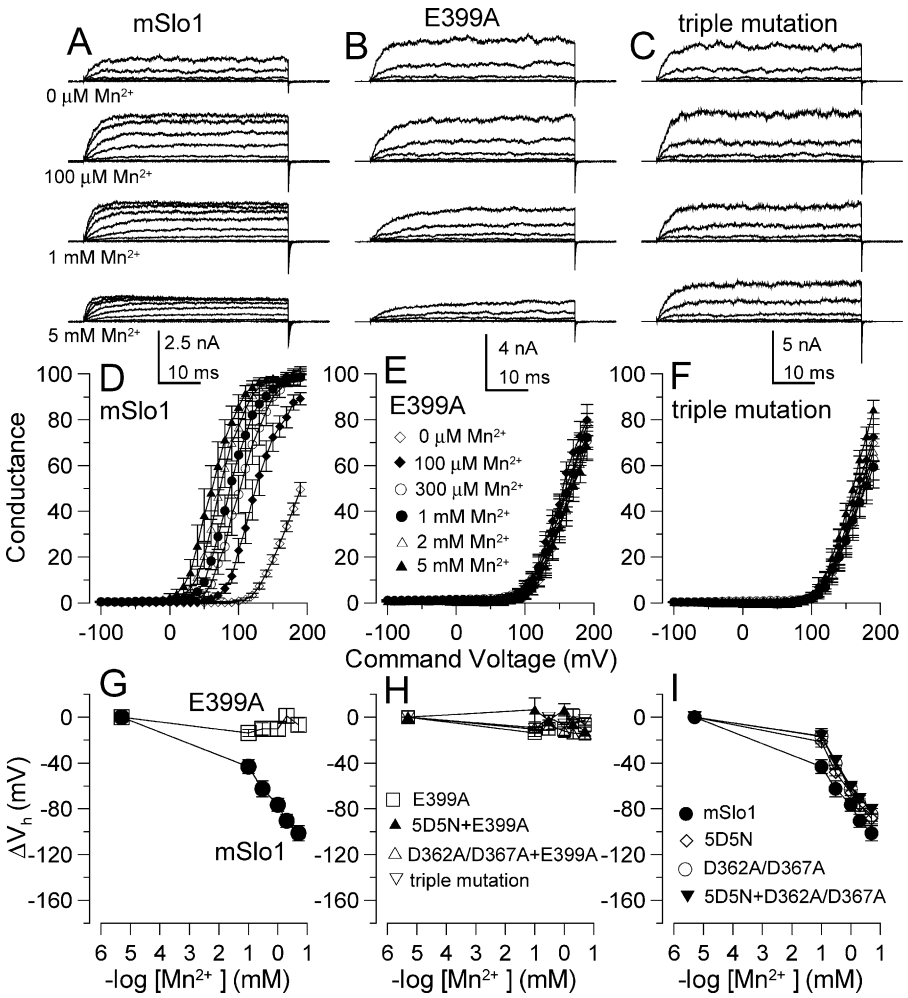

FIGURE 2. The ability of Mn^{2+} to activate BK current depends on the E399 low affinity site. (A–C) Currents resulting from Slo1 (A), E399A (B), and the triple mutation (C, 5D5N + D362AD367A + E399A) were activated as in Fig. 1. (D–F) G–V curves were generated over $[Mn^{2+}]_i$ from 0 to 5 mM for Slo1 (n = 6), E399A (n = 5), and the triple mutation (n = 5). Open diamonds, 0 μM; filled diamonds, 100 μM; open circles, 300 μM; filled circles, 1 mM; open triangles, 2 mM; filled triangles, 5 mM. (G) Activation ΔV_h is plotted versus $[Mn^{2+}]_i$ for Slo1 (n = 6) and E399A (n = 5). (H) Activation ΔV_h is plotted versus $[Mn^{2+}]_i$ for mutants containing E399A (5D5N + E399A, n = 4; D362A/D367A + E399A, n = 6; triple mutation, n = 5). (H) Activation ΔV_h is plotted versus $[Mn^{2+}]_i$ for Slo1 and mutants not containing E399A (5D5N, n = 5; D362A/D367A, n = 7; 5D5N + D362A/D367A, n = 8).

change in voltage dependence (Fig. 2 D). The negative V_h shift produced by 5 mM Mn^{2+} relative to 0 divalent is >100 mV (Fig. 2 G), while 100 μM Mn^{2+} produces an ~50-mV leftward shift. Mutation of the low affinity site alone is sufficient to abolish most of the effect of Mn^{2+} (Fig. 2, E and G). Moreover, additional mutation of the two high affinity sites together with E399A does not produce any additional effect other than that caused by E399A alone (Fig. 2, F and H). In fact, Mn^{2+} loses its ability to activate current only for those constructs in which the E399A mutation is present (Fig. 2 H), while Mn^{2+} produces similar current activation for all constructs containing an intact E399 site (Fig. 2 I). These results show clearly that Mn^{2+} modulates BK channels predominantly through the low affinity site. Furthermore, although we were only able to examine Mn^{2+} concentrations up through 5 mM, the E399A mutation appears to completely remove the approximately −90-mV shift produced by 5 mM Mn^{2+}, whereas E399A removes about half of the approximately −60-mV shift caused by 10 mM Mg^{2+} (Xia et al., 2002).

The cumulative data in Fig. 2 I suggest that mutation of either 5D5N or D362A/D367A alone may produce a small reduction in the ability of Mn^{2+} to shift activation at 100 μM Mn^{2+}, raising the possibility of a small effect involving the higher affinity Ca^{2+} regulatory mechanisms. However, these small effects of 5D5N and D362A/D367A do not appear to be additive, and estimates of V_h for constructs with very positive V_h are subject to uncertainties (Fig. 2 I). Furthermore, simultaneous mutation of all three sites (the triple mutation: 5D5N/D362AD367A/E399A) shows a behavior similar to E399A alone (Fig. 2 H). Although we cannot completely exclude the possibility that Mn^{2+} may produce a small activation effect through one or both of the higher affinity sites, it is clear that in comparison to Ca^{2+} or Cd^{2+}, the ability of Mn^{2+} to shift activation via these sites is either absent or markedly reduced.

The E399 Low Affinity Site Is Partially Responsible for the Ability of Ni^{2+} and Co^{2+} To Activate BK Channels

We next tested the selectivity of the three sites for Ni^{2+}. In contrast to its effects on activation by Mn^{2+}, the E399A mutation reduces, but does not fully abolish, the negative V_h shifts caused by Ni^{2+} on mSlo1, which is

about −160 mV with 50 mM Ni^{2+} (Fig. 3 A). However, simultaneous mutation of the two high affinity sites has no effect on the ability of Ni^{2+} to produce V_h shifts (Fig. 3 B). The important role of E399 in the effects of Ni^{2+} is also supported by the fact that all constructs containing E399A exhibit Ni^{2+}-induced shifts in V_h similar to those seen in E399A alone (Fig. 3 C). Furthermore, all constructs containing wild-type E399 exhibit Ni^{2+}-induced V_h shifts similar to that of wild-type mSlo1 (Fig. 3 D).

The experimental results from Co^{2+} are similar to those with Ni^{2+} (Fig. 3, E–H). In brief, 20 mM Co^{2+} produces an ~150-mV negative V_h shift of mSlo1 BK channels (Fig. 3 E). All constructs containing E399A show a V_h–$[Co^{2+}]$ relationship similar to that of the E399A mutant, in which the ability of Co^{2+} to produce a V_h shift is partially removed (Fig. 3, E and G). Single or double mutation of high affinity sites does not change the V_h shifts caused by Co^{2+} on BK channels (Fig. 3, F and H).

The results from Ni^{2+} and Co^{2+} suggest that, among the previously defined three divalent cation regulatory mechanisms, only the E399 low affinity site contributes appreciably to the activation effect conferred by Ni^{2+} and Co^{2+}. However, it should be noted that for both mM Ni^{2+} and Co^{2+} some ability to shift V_h persists even after mutation of E399, similar to the effects of Mg^{2+}, but distinct from that of Mn^{2+}.

Activation of BK Channels by Sr^{2+} Involves All Three Divalent Cation Regulatory Sites

Representative current traces from wild-type mSlo1, D362A/D367A+E399A, D362A/D367A, and E399A over a range of $[Sr^{2+}]$ are shown in Fig. 4 (A–D). For $[Sr^{2+}]$ >300 μM, a strong voltage-dependent block was observed that influenced current estimates for both steady state and tail currents for all tested constructs. At very positive potentials, Sr^{2+} produces a slow, time-dependent blockade that can result in complete block of steady-state current. Unblock following repolarization is sufficiently slow that only partial recovery from block is observed during tail currents. Intriguingly, at higher $[Sr^{2+}]$ and strong depolarizations, the tail current G–V curves show an unusual N shape, which cannot be simply described by a combination of activation and blocking processes (Fig. 4, E and F). Previous work has demonstrated that Sr^{2+} reduces BK current both by slow and fast blocking mechanisms probably involving two different positions of occupancy within the pore (Sugihara, 1998). How these two different facets of Sr^{2+} block may relate to the apparent N shape seen here is not clear. However, the N shape phenomenon is suggestive of a presumed punchthrough mechanism (Nimigean and Miller, 2002), in which depolarization might drive the blocking ion through the ion channel. An alternative explanation has also been suggested in

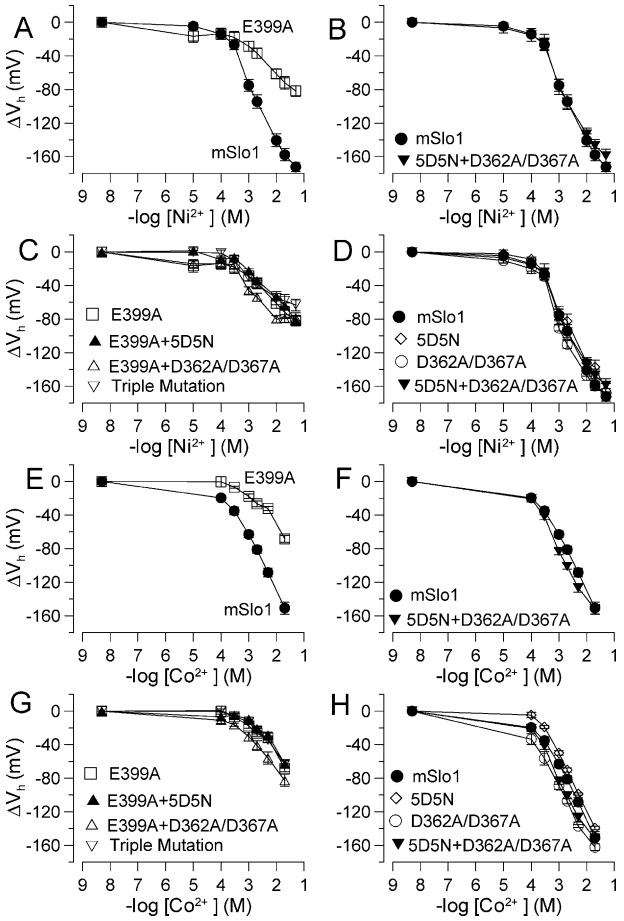

FIGURE 3. Effects of Ni^{2+} and Co^{2+} are disrupted by the E399A mutation. (A) Activation ΔV_h is plotted as a function of $[Ni^{2+}]_i$ for Slo1 ($n = 4$) and E399A ($n = 6$). (B) Activation ΔV_h is plotted as a function of $[Ni^{2+}]$ for Slo1 and the construct with mutation of both high affinity sites (5D5N + D362A/D367A, $n = 5$). (C) Activation ΔV_h is plotted as a function of $[Ni^{2+}]_i$ for all mutants containing E399A (5D5N + E399A, $n = 6$; D362A/D367A + E399A, $n = 5$; triple mutation, $n = 6$). (D) Activation ΔV_h is plotted as a function of $[Ni^{2+}]$ for all constructs with an intact E399 (5D5N, $n = 5$; D362A/D367A, $n = 9$; 5D5N + D362A/D367A, $n = 5$). (E–H) Activation ΔV_h is plotted as a function of $[Co^{2+}]$ for combinations of constructs identical to those in A–D. mSlo1, $n = 5$; 5D5N, $n = 5$; D362A/D367A, $n = 4$; E399A, $n = 4$; 5D5N + D362A/D367A, $n = 5$; 5D5N + E399A, $n = 6$; D362A/D367A + E399A, $n = 5$; triple mutation, $n = 4$.

recent work pointing out that an apparent punchthrough phenomenon may arise from interactions between blocker and permeant ions with the permeation pathway (Heginbotham and Kutluay, 2004).

Because of the N shape of the G–V curves with Sr^{2+}, we were unable to define curves reflecting solely the ability of Sr^{2+} to activate BK channels. Manipulations of stimulation protocols such as prolongation of the time between sweeps, varying the activation step duration, or changing the tail current potential had minimal effect on the essential properties of the tail current G–V curves. As a consequence, here we simply show the rela-

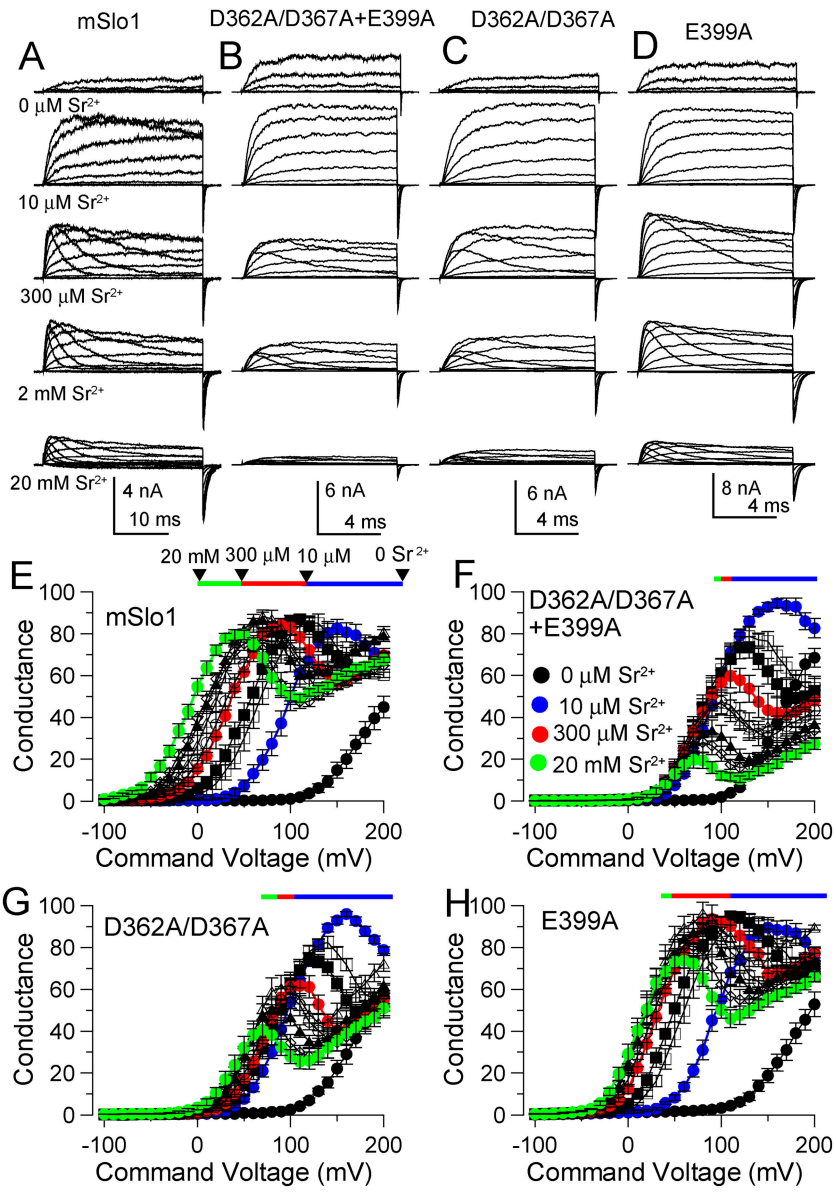

FIGURE 4. Sr^{2+} activates BK channels through all three mutationally defined sites. (A) Current activation by Sr^{2+} for Slo1 is shown for voltages up to +200 mV. Note the slow voltage-dependent block at $[Sr^{2+}]$ of 300 μM and higher. (B) Currents activated by Sr^{2+} in construct D362A/D367A+E399A are shown. Note the faster time based in B–D, in comparison to A. (C) Currents activated by Sr^{2+} in construct D362A/D367A are shown. (D) Currents activated by Sr^{2+} in channels containing the E399A mutation are shown. The stimulation protocol was similar to that in Fig. 1. (E–H) G–V curves were generated over $[Sr^{2+}]_i$ from 0 to 20 mM for wild-type Slo1 (E, $n = 7$), the mutant with only the intact Ca^{2+} bowl region (D362A/D367A + E399A, F, $n = 7$), D362A/D367A (G, $n = 7$), and E399A (H, $n = 5$). $[Sr^{2+}]_i$ are as follows: filled circles, 0 μM; filled blue circles, 10 μM; open squares, 50 μM; filled squares, 100 μM; filled red circles, 300 μM; open circles, 1 mM; open triangles, 2 mM; filled triangles, 5 mM; open diamonds, 10 mM; filled green circle, 20 mM. G–V amplitudes were normalized to the maximal current amplitude at 10 μM Sr^{2+}. The colored horizontal bar indicates the approximate shift in the G–V curve for increases in Sr^{2+} from 0 to 10 μM (blue), 10 to 300 μM (red), 300 μM to 20 mM (green), corresponding approximately to the contribution of the Ca^{2+} bowl (blue), D362/D367 (red), and E399 (green) to the effect of Sr^{2+}.

tive tail current G–V shifts among various Sr^{2+} concentrations. G–V curves were normalized to the conductance at 10 μM Sr^{2+} for each patch. Relative shifts were measured at the nominal half activation position. We must emphasize that, because of the blocking effects and the possibility that channel opening has not reached saturation at 10 μM Sr^{2+}, the real maximum conductance activated by 300 μM Ca^{2+} is much larger than the peak conductance shown in these figures. Despite the uncertainties involved in determining the true V_h for activation in Sr^{2+}, the relative ability of Sr^{2+} to shift gating in different constructs seems readily apparent.

For wild-type mSlo1, there are significant shifts in the G–V curves between $[Sr^{2+}]$ of 0 to 10 μM (blue bars), 10 to 300 μM (red bars), and 300 μM to 20 mM (green bars) (Fig. 4 E). For D362A/D367A+E399A, in which only the calcium bowl site is intact, the relative shift between 0 to 10 μM Sr^{2+} is similar to the shift in G–V seen in mSlo1, but little additional shift is observed between 10 μM to 20 mM Sr^{2+} (Fig. 4 F). This result indicates that the calcium bowl is mainly responsible for the effect of Sr^{2+} <10 μM.

When only the D362/D367 residues are mutated, the relative G–V shift between 10 and 300 μM Sr^{2+} is substantially reduced compared with mSlo1 (Fig. 4 G). In contrast, with the E399A mutation alone, only the relative shift between 300 μM and 20 mM Sr^{2+} is significantly decreased, with little change in the shifts that occur over the range of 0 to 300 μM Sr^{2+} (Fig. 4 H). These results suggest that the D362/D367 site accounts for Sr^{2+} effects from 10 to 300 μM, and E399 participates in a low affinity effect of Sr^{2+}.

Because the calcium bowl accounts for Sr^{2+} effects at 10 μM Ca^{2+} and below, constructs in which the calcium

bowl is mutated require higher Sr^{2+} before activation is observed. As a consequence, for constructs containing the 5D5N mutations, the severe blocking effects of Sr^{2+} at the voltages required for activation precluded our ability to study such constructs. Despite this limitation, the available results all support the conclusion that, similar to Ca^{2+}, Sr^{2+} activates BK channels through all three divalent cation regulatory mechanisms.

One final aspect of the effects of Sr^{2+} requires mention. In both construct D362A/D367A and also D362A/D367A+E399A, there appears to be a more robust block of tail currents than in either wild-type Slo1 or in E399A, when compared at a voltage (e.g., +100 to +150 mV) where 10 μM Sr^{2+} appears to produce near maximal activation. This difference occurs despite the fact that both the onset of block by Sr^{2+} at these voltages and recovery from block at more negative potentials is largely similar for all constructs. This suggests that the voltage- and time-dependent block by Sr^{2+}, probably involving pore blockade, does not differ among the constructs. Yet there appears to be an additional reduction in relative tail current amplitude at higher Sr^{2+} that may not be explained solely by such a block. At present, we do not have an explanation for the additional blockade produced in constructs containing the D362A/D367A mutations.

In sum, each of the three mutationally defined regulatory mechanisms exhibits a unique profile of sensitivity to divalent cations. The E399A mutation defines a process that is acted upon by all divalent cations we have examined. The D362A/D367A mutations participate in a mechanism that can be regulated by Ca^{2+}, Cd^{2+}, and Sr^{2+}, while activation mediated by the Ca^{2+} bowl only occurs with Ca^{2+} and Sr^{2+}.

The Three Regulatory Sites Affect Channel Gating Kinetics in Distinct Ways

Despite the number of distinct kinetic states that are hypothesized to contribute to BK channel gating (Rothberg and Magleby, 1999, 2000; Zhang et al., 2001; Horrigan and Aldrich, 2002), the kinetic relaxations associated with BK current activation and deactivation are remarkably simple, being reasonably well characterized by a single exponential time course (Horrigan and Aldrich, 2002). Increases in $[Ca^{2+}]$ typically increase current activation rate, up to some limiting activation rate at high $[Ca^{2+}]$ (Zhang et al., 2001). In contrast, increases in $[Ca^{2+}]$ slow deactivation, with little hint of any limiting deactivation rate even at mM Ca^{2+} or Mg^{2+} (Zhang et al., 2001). The existence of a single primary kinetic relaxation in the gating behavior of BK channels has been generally explained by the idea that the rate-limiting relaxation in the gating process is a central closed–open equilibrium (C-O) (Horrigan and Aldrich, 2002).

Given that three distinct divalent cation-dependent mechanisms appear to regulate BK gating, here we evaluate whether any of these mechanisms are associated with distinct effects on channel gating kinetics. Because Ca^{2+} interacts with both high affinity sites and Mg^{2+} only acts at the low affinity site (Shi and Cui, 2001; Zhang et al., 2001; Shi et al., 2002; Xia et al., 2002), we have compared gating behavior at 0, 1, 10, and 300 μM Ca^{2+} to examine the kinetic roles of the calcium bowl and D362/D367 residues, while 20 mM Mg^{2+} was applied to evaluate the kinetic effects of the E399 residue.

Fig. 5 (A and B) shows example traces used for measurement of activation and deactivation time course from wild-type mSlo1 at different $[Ca^{2+}]$. Voltage commands ranged from −180 to +190 mV for activation and from +180 to −180 mV for deactivation. For mSlo1, deactivation slows with increases in $[Ca^{2+}]$, while activation is accelerated as $[Ca^{2+}]$ is elevated over the range of 1 to 300 μM (Fig. 5 C). At positive activation potentials, there is also an unusual slowing of activation at 1 μM Ca^{2+} relative to 0 Ca^{2+} (Fig. 5 C), which has been noted in previous work (Zhang et al., 2001).

For channels in which the calcium bowl is mutated (5D5N), the increase in activation rate between 0 and 10 μM Ca^{2+} is largely reduced (compare sample traces on the right of Fig. 5, C and D), while the deactivation process is less strongly influenced by Ca^{2+} bowl mutation at Ca^{2+} up to 300 μM (Fig. 5, compare C with D). In contrast, for channels with simultaneous mutation of D362A/D367A+E399A, such that only the calcium bowl site is functional, the increase in activation rate between 0 and 10 μM Ca^{2+} is comparable with that in wild-type mSlo1 BK channels (Fig. 5, compare C with E). Yet, in this construct, the increase in activation rate between 10 and 300 μM Ca^{2+} and the slowing of deactivation is almost abolished (Fig. 5 E). These results convincingly demonstrate that the main kinetic contribution of the calcium bowl is to increase the activation rate for <10 μM Ca^{2+}, while the Ca^{2+} bowl plays little role in effects of Ca^{2+} on deactivation.

In contrast, for channels in which the D362/D367 site alone is mutated, increases in $[Ca^{2+}]$ from 0 to 300 μM produce only a small slowing of deactivation in marked contrast to wild-type Slo1 (compare Fig. 6 A with Fig. 5 C). Similarly, the increase in activation rate seen in wild-type Slo1 between 10 and 300 μM Ca^{2+} is also largely reduced by the D362A/D367A mutation (Fig. 6 A). On the other hand, for channels in which only the D362D367 site is functional (e.g., 5D5N+E399A; Fig. 6 B), the extent of slowing of deactivation produced by Ca^{2+} up through 300 μM and the acceleration of activation between 10 and 300 μM Ca^{2+} are comparable with those in mSlo1 (compare Fig. 5 C with Fig. 6 B). Consistent with these observations, 300 μM Ca^{2+} confers little kinetic effect on channels in

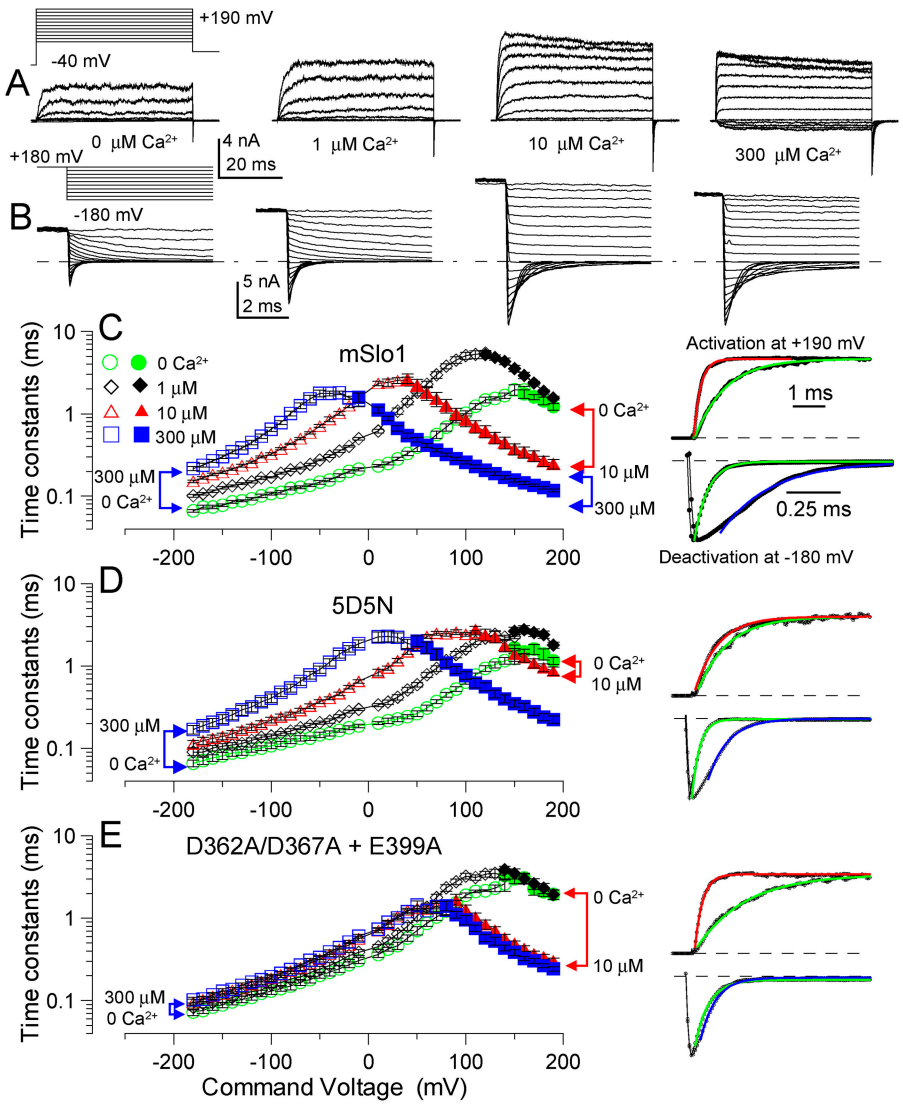

FIGURE 5. The calcium bowl is mainly responsible for the acceleration of activation from 0 to 10 mM Ca^{2+}. (A) Typical currents used for measurement of current activation time constants are shown for mSlo1 with 0, 1, 10, and 300 μM Ca^{2+} along with the voltage activation protocol. (B) Examples of Slo1 tail currents used for measurement of deactivation time constants are given for the indicated [Ca^{2+}]. Voltage steps were from −180 to +180 mV in 20-mV increments (only every 40 mV is shown in the displayed protocol). (C) Activation (filled symbols) and deactivation (open symbols) time constants for Slo1 (n = 6) are plotted at various [Ca^{2+}] showing the slower deactivation and faster activation produced by Ca^{2+}. Traces on the right (top pair of traces) show normalized current activation at +190 mV with 0 μM Ca^{2+} (green line is fitted single exponential, 1.00 ms) and 10 μM Ca^{2+} (red fitted exponential, 0.227 ms). Bottom pair of right-hand traces show current deactivation at −180 mV for 0 μM Ca^{2+} (green fitted line, 0.041 ms) and 300 μM Ca^{2+} (blue fitted line, 0.107 ms). Both activation and deactivation examples are from the same patch. For activation time courses, only every 10th digitized current value is displayed. (D) Time constants are plotted as in C, but for 5D5N (n = 6). Traces on the right are identical in format to those in C. Activation τ: 0 Ca^{2+}, 0.996 ms; 10 μM Ca^{2+}, 0.771 ms. Deactivation t: 0 Ca^{2+}, 0.041 ms; 300 μM Ca^{2+}, 0.107 ms. (E) Time constants are plotted as in C, but for D362A/D367A + E399A (n = 8). Activation τ: 0 Ca^{2+}, 1.61 ms; 10 μM Ca^{2+}, 0.254 ms. Deactivation τ: 0 Ca^{2+}, 0.074 ms; 10 μM Ca^{2+}, 0.080 ms.

which both high affinity sites are mutated simultaneously (5D5N/D362AD367A; Fig. 6 C). Taken together, these results indicate that the D362/D367 site is primarily responsible not only for the slowing of deactivation caused by Ca^{2+} up through 300 μM, but also for the acceleration of activation from 10 to 300 μM Ca^{2+}. Thus, the Ca^{2+} bowl site and the D362/D367A site each influence distinct kinetic aspects of BK channel function. It should also be noted that the slight slowing of activation that is observed in wild-type Slo1 by increases in Ca^{2+} from 0 to 1 μM appears to be absent in constructs containing the D362A/D367A mutations.

Mg^{2+}, which enhances BK channel activation through the E399 low affinity site (Shi et al., 2002; Xia et al., 2002), only contributes to a slowing of deactivation of Slo1, with little effect on the activation kinetics of channel gating (Fig. 7 A). The slowing of deactivation is completely abolished in channels with the E399A mutation (Fig. 7 B). Therefore, the mechanism of channel regulation involving the low affinity Mg^{2+} site involves a slowing of deactivation, with little effect on activation. This conclusion is also supported by the properties of the construct in which the E399 site is intact, but both higher affinity sites are mutated, i.e, 5D5N+D362A/D367A. In the absence of the two high affinity sites, Mg^{2+} exerts the same effects on channel gating behavior as on wild-type BK channels (Fig. 7 C). Thus, the slowing of deactivation exerted by mM Mg^{2+} or Ca^{2+} is disrupted solely by mutation of the E399 residue.

DISCUSSION

The main conclusions of this work are the following. (1) The calcium bowl site is activated by Ca^{2+} and Sr^{2+},

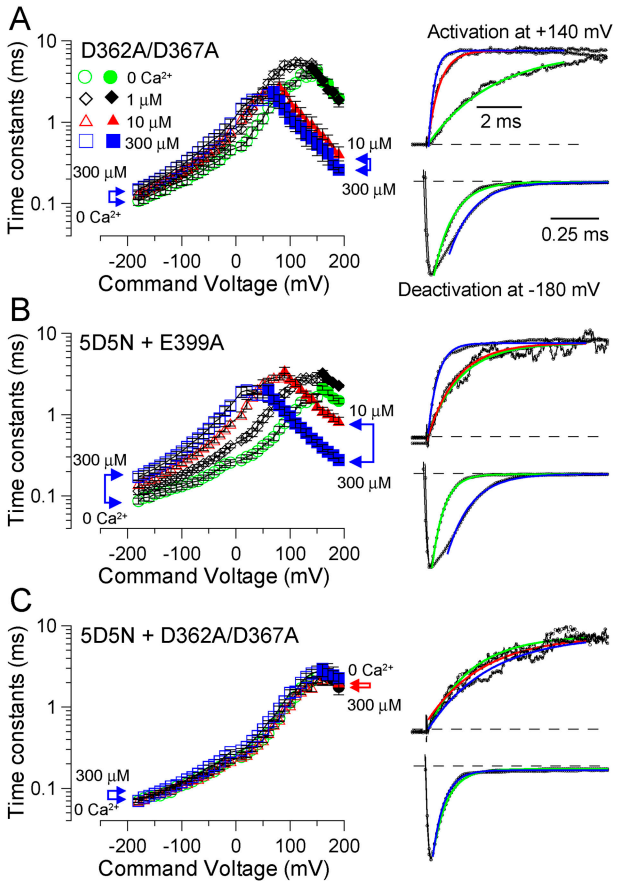

FIGURE 6. The D362/D367 site slows deactivation and accelerates activation in the range of 10 to 300 μM Ca^{2+}. Activation and deactivation time courses were determined as in Fig. 5 at 0, 1, 10, and 300 μM Ca^{2+}. (A) Effects of Ca^{2+} on activation and deactivation time constants are plotted as a function of command voltage for D362A/D367A (n = 6). Open symbols were measured from deactivation protocols and filled symbols from activation protocols. Representative normalized current traces for activation (at +190 mV) and deactivation (at −180 mV) are shown on the right, along with lines showing single exponential fits. Activation time constants: 0 Ca^{2+} (green), 1.74 ms; 10 μM Ca^{2+} (red), 0.34 ms; 300 μM Ca^{2+} (blue), 0.27 ms. Deactivation time constants: 0 Ca^{2+} (green), 0.104 ms; 300 μM Ca^{2+} (blue), 0.129 ms. (B) Time constants for the construct with both the Ca^{2+} bowl and E399 mutated (5D5N+E399A; n = 7) are plotted with representation current traces and fitted exponentials on the right. Activation time constants: 0 Ca^{2+}, 1.22 ms; 10 μM Ca^{2+}, 0.74 ms; 300 μM Ca^{2+}, 0.26 ms. Deactivation time constants: 0 Ca^{2+}, 0.065 ms; 300 μM Ca^{2+}, 0.130 ms. (C) The dependence of activation and deactivation time constants is plotted at various Ca^{2+} for the construct with both higher affinity sites mutated (5D5N+D362A/D367A, n = 6) with sample traces and fitted single exponentials on the right. Activation time constants: 0 Ca^{2+}, 1.69 ms; 10 μM Ca^{2+}, 1.67 ms; 300 μM Ca^{2+}, 2.91 ms. Deactivation time constants: 0 Ca^{2+}, 0.079; 300 μM Ca^{2+}, 0.631 ms.

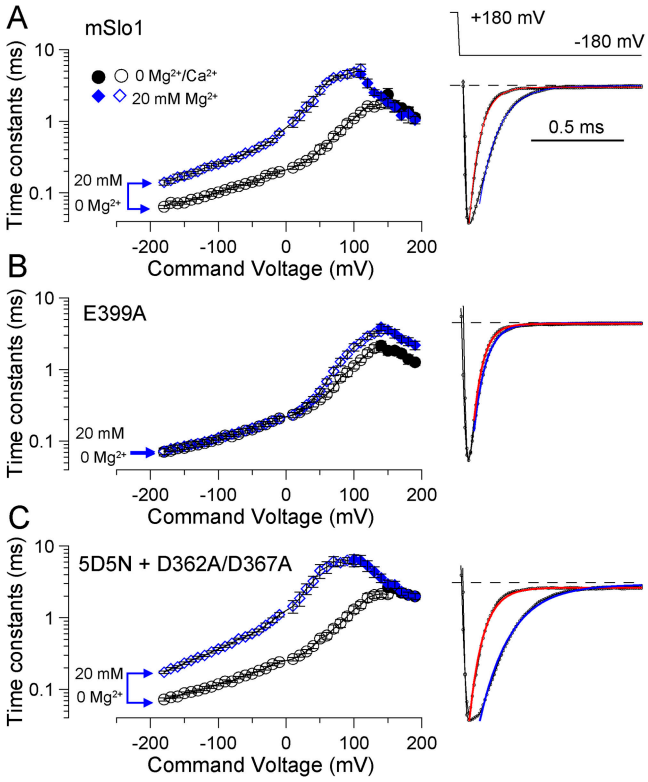

FIGURE 7. The E399 low affinity site slows deactivation. Activation and deactivation time courses were determined as in Fig. 5 but either in the absence or presence of 20 mM Mg^{2+}. (A) Effect of 20 mM Mg^{2+} on activation time constants or deactivation time constants in wild-type Slo1 (n = 6). Open symbols, deactivation; filled symbols, activation. Traces on the right show normalized deactivation currents at −180 mV with either 0 Mg^{2+} (red fitted line, 0.061 ms) or 20 mM Mg^{2+} (blue fitted line, 0.107 ms). (B) Effect of 20 mM Mg^{2+} on activation and deactivation time constants with the E399A mutation (n = 7). Traces on the right are as in A. τ_d: 0 μM Mg^{2+}, 0.055 ms; 20 mM Mg^{2+}, 0.066 ms. (C) Effect of 20 mM Mg^{2+} in the construct with both higher affinity sites mutated (5D5N+D362A/D367A; n = 7). Traces on the right are as in A. τ_d: 0 μM Mg^{2+}, 0.076 ms; 20 mM Mg^{2+}, 0.170 ms. Circles, 0 μM Mg^{2+}; diamonds, 20 mM Mg^{2+}.

but not Cd^{2+} or smaller divalent cations. Disruption of this site has little effect on current deactivation, but this site plays a role in Ca^{2+}-dependent increases in activation rate <10 μM Ca^{2+}. (2) The D362/D367-related site is activated by Ca^{2+}, Sr^{2+}, and Cd^{2+}, but not smaller divalent cations. This site contributes to a slowing of deactivation produced by Ca^{2+} up to 300 μM, and it also contributes to Ca^{2+}-dependent increases in activation rate between 10 and 300 μM Ca^{2+}. (3) The E399 low affinity site plays a role in slowing of deactivation, without affecting activation; this site can be activated by all the divalent cations tested. Overall the results suggest that mutation of a given regulatory site has largely similar effects irrespective of whether either of the other two sites are functional. The unique divalent cation selectivity of these regulatory mechanisms supports the existence of three distinct divalent cation binding sites. Moreover, the specific kinetic effects of each mechanism imply that these mechanisms act in independent ways to regulate BK channels.

At Least Three Divalent Cation Binding Sites Regulate BK Gating

The possible presence of two RCK domains associated with each BK α subunit (Jiang et al., 2002; Roosild et al., 2004) naturally suggests that a Ca^{2+} regulatory site on each RCK domain on a single BK channel α subunit may be required for proper function of the cytosolic structure of the BK channel. As summarized in INTRODUCTION, mutational analyses have supported this idea that two distinct Ca^{2+}-dependent regulatory mechanisms sensitive to μM Ca^{2+} may participate in BK channel regulation. For the Ca^{2+} bowl regulatory mechanism, Ca^{2+} binding studies to fusion peptides containing the Ca^{2+} bowl (Bian et al., 2001; Braun and Sy, 2001) and more detailed mutagenesis in conjunction with both physiological and binding assays (Bao et al., 2004) have bolstered the idea that the Ca^{2+} bowl does, in fact, represent a likely Ca^{2+} binding site. However, for the high affinity mechanism identified by D362AD367A (or M513), no specific evidence supports the idea that any of these residues participate in coordination of Ca^{2+} ions. Based on mutagenesis alone, it has remained a possibility that each α subunit contains only a single Ca^{2+} binding site, but that mutations at different positions in the COOH terminus can disrupt independently acting components of the regulatory apparatus.

To provide independent evidence that each mutationally defined regulatory effect corresponds to a distinct divalent cation binding site, the present results have shown that each higher affinity Ca^{2+} regulatory site exhibits a unique profile of divalent cation sensitivity. An important point is that, for either the 5D5N mutations or D362AD367A mutations, the consequences of a given mutation are the same, irrespective of whether other sites are simultaneously mutated. This argues against the possibility that there is only a single high affinity site that exhibits altered binding/selectivity properties after mutation. Furthermore, the results suggest that the particular profile of divalent cation sensitivity observed for each putative regulatory mechanism reflects the intrinsic properties of a unique binding site and that each site acts largely independently of each other. Thus, two distinct higher affinity Ca^{2+} binding sites on each Slo1 α subunit contribute to regulation of BK channels by divalent cations. The specific residues that coordinate ion binding for each of these sites remain to be identified.

The presence of two higher affinity Ca^{2+} regulatory domains in each α subunit supports the idea that COOH terminus involves a modular structure with a Ca^{2+}-dependent regulatory site in association with each of the two RCK domains. The D362D367 residues are, in fact, positioned in the first BK RCK domain within loops homologous to those known to contain ligand coordinating residues in the RCK domains of bacterial K^+ channels (Jiang et al., 2001). The position of the Ca^{2+} bowl with respect to the hypothesized second RCK domain is less clear, but is consistent with the idea that a second RCK-containing module in the BK channel COOH terminus also contains a Ca^{2+}-binding site that regulates channel gating. Intriguingly, the idea that the cytosolic structure of each BK channel α subunit contains two modular elements, perhaps similar to the MthK bacterial channel (Jiang et al., 2002), was supported by earlier work indicating that functionally normal channels could arise from the separate expression of cDNA encoding a peptide corresponding to the second RCK domain (and Ca^{2+} bowl) along with cDNA encoding a peptide corresponding to the first RCK domain attached to the pore module (Wei et al., 1994). The point of separation between the two components of the COOH terminus in these earlier experiments was essentially a linker between the two RCK domains.

The present results also suggest that there is a second low affinity site in addition to that defined by E374 and E399. Even at 10 mM Mg^{2+}, an appreciable V_h shift (~20–30 mV) is still observed with either the E374A (Shi et al., 2002) or E399A (Xia et al., 2002) mutations. Here, following mutation of E399, similar residual shifts were observed with mM concentrations of Ni^{2+} and Co^{2+}. Furthermore, with the E399A mutation, effects of Ni^{2+} and Co^{2+} were observed at concentrations even as low as 1 mM, despite the fact that neither cation has appreciable effects on the higher affinity sites, suggesting the presence of an additional low affinity site. Given that the E399A mutation completely abolishes the effects of 5 mM Mn^{2+}, this putative second low affinity site may exhibit a selectivity distinct from that of E399. Thus, whatever the basis for the residual effect of mM concentrations of divalent cations following mutation of E399, there are probably specific residues on the BK α subunit that mediate this effect.

Defining the Ion Selectivity of an Allosteric Regulatory Site

A previous study (Oberhauser et al., 1988) of skeletal muscle BK channels in bilayers reported that Ca^{2+}, Cd^{2+}, Sr^{2+}, Mn^{2+}, Fe^{2+}, and Co^{2+} were effective at activating channels while Mg^{2+}, Ni^{2+}, Ba^{2+}, Cu^{2+}, Zn^{2+}, Hg^{2+}, and Sn^{2+} were ineffective. However, Ni^{2+} and Mg^{2+}, when studied in the presence of Ca^{2+}, produced an additional enhancement of activation, while Ba^{2+}, Cu^{2+}, Zn^{2+}, Hg^{2+}, and Sn^{2+} remained ineffective. These results were interpreted in terms of two kinds of effects: first, direct channel activation at a Ca^{2+} activation site and, second, an allosteric effect mediated by some divalent cations that enhanced the effectiveness of Ca^{2+}. Now, within the three binding site perspective, those cations that were observed to cause activation (Oberhauser et al., 1988) correspond either to those acting on one or both of the high affinity sites (Ca^{2+}, Sr^{2+}, and

TABLE I

Activation Effectiveness of Divalent Cations on Slo1

	Radius (A) (Pauling, 1960)	Activation effect[a]	Ca^{2+} bowl-sensitive V_h shift[c]	D362/D367-sensitive V_h shift[d]	E399A-sensitive V_h shift[e]	V_h shift remaining in triple mutation[f]
Sr^{2+}	1.13	3	~80 mV	~50 mV	~25 mV (10 mM)	
Ca^{2+}	0.99	1	~80 mV[b]	~120 mV[b]	~55 mV (10 mM)[b]	+50 mV (10 mM)[b]
Cd^{2+}	0.97	2	<10 mV (0–100 μM)	~120 mV (0–100 μM)	60 mV (300 μM)	0 mV (300 μM)
Mn^{2+}	0.80	4	<10 mV (0–5 mM)	<10 mV (0–5 mM)	~90 mV (5 mM)	0 mV (5 mM)
Co^{2+}	0.74	5	<20 mV (0–500 μM)	<10 mV (0–500 μM)	80 mV (5 mM)	30 mV (5 mM)
Mg^{2+}	0.65	Ineffective	0 mV[b]	0 mV[b]	~55 mV (10 mM)[b]	~35 mV (10 mM)[b]
Ni^{2+}	0.72	Ineffective	<10 mV (0–500 μM)	<10 mV (0–500 μM)	80 mV (10 mM)	60 mV (10 mM)

[a]Oberhauser et al., 1988.

[b]Xia et al., 2002.

[c]Estimates based on the reduction in the V_h shift produced in the 5D5N mutation relative to parent constructs without mutation of the five aspartates.

[d]Estimates based on the reduction in the V_h shift produced by the D362A/D367A mutations.

[e]Estimates based on the reduction in the V_h shift produced by the E399A mutation.

[f]Remaining V_h shift in the triple mutation at the indicated concentrations.

Cd^{2+}) or to those (Mn^{2+} and Co^{2+}) that were studied at concentrations at which effects on the low affinity site would begin to be observed. Here, because of higher concentrations and more positive activation potentials, Mg^{2+} and Ni^{2+} were also observed to activate channels directly through the lower affinity site.

Our results also support the earlier conclusion (Oberhauser et al., 1988) that selectivity for channel activation is correlated with cation size. The Ca^{2+} bowl interacts with the two largest cations we have examined, Ca^{2+} and Sr^{2+}. The D362/D367 site interacts with the three largest cations (Ca^{2+}, Sr^{2+}, and Cd^{2+}), while the lower affinity site interacts with all cations we have examined. On the other hand, the differential effects of Ca^{2+} and Cd^{2+} on the Ca^{2+} bowl points out that size per se is not sufficient for defining the effects of a given cation, but that other physico-chemical properties of a given ion are important. Yet, the fundamental importance of ionic radius is clear and, in general, it is the case that the binding sites of greater specificity are those that prefer ions of larger radii. This seems somewhat surprising, given that, in a site preferring larger ions, ions of smaller radii are also likely to pass in and out of the general coordinates of that site. Two factors may contribute to the lack of effect of smaller ions. One possibility is that, similar to one model of ion permeation (Doyle et al., 1998), precise coordination distances between ion occupancy positions and oxygen donors may be critical for defining the residence time of an ion at a given site. Thus, the specific chemical nature and resulting strength of interactions between a given divalent cation and ion-coordinating residues would impact on this residence time. A second factor is that our analysis compares selectivity for activation, and not selectivity for binding. When selectivity is being compared by a measurement of a response that depends on an allosteric mechanism, the ability of a cation to cause activation depends not only on its ability to occupy the binding site, but also on its ability to bind more tightly to the open state of the channel. This latter point is, in fact, the crux of the idea of allosteric regulation. The measurements used here provide no direct information about the ability of any given ion to occupy the presumed binding sites, except as indicated indirectly by current activation. Thus, some cations might effectively occupy a binding site, but exhibit no difference in binding between closed and open conformations. Cations acting in such a fashion would be expected to exert inhibitory effects on activation by Ca^{2+}.

An interesting case is the apparent lack of effect of Cd^{2+} on the Ca^{2+} bowl site, despite their similarity in ionic radii (Table I). Does Cd^{2+} act as a blocker of the Ca^{2+} bowl site? Although specific experiments to test this possibility will need to be done, some aspects of the data seem consistent with this possibility. In the D362A/D367A construct containing a functional Ca^{2+} bowl, Cd^{2+} produces a small rightward shift in the G–V curve at 100 μM (Fig. 1 E). One interpretation of such an effect is that Cd^{2+} may bind with reasonable affinity to the binding site corresponding to calcium bowl, but the binding affinity is slightly higher in the closed state than in open state. Despite their similarity in ionic radii, it has been noted that Ca^{2+} and Cd^{2+} differ appreciably in their coordination chemistry (Oberhauser et al., 1988), with Ca^{2+} more likely to form ionic bonds with carboxyl and carbonyl groups, whereas Cd^{2+} has a higher affinity for nitrogen and sulfur moieties. Perhaps the Ca^{2+} bowl lacks the groups appropriate for tighter binding of Cd^{2+} to the open channel conformation. Experiments that examine competition between Cd^{2+} and Ca^{2+} in particular constructs might illuminate this issue.

Similar considerations to those just mentioned pertain to evaluation of the selectivity of the site defined by the D362/D367 residues. The D362/D367 related site responds to Ca^{2+}, Cd^{2+}, and Sr^{2+}, but not appreciably to four cations, Ni^{2+}, Co^{2+}, Mn^{2+}, and Mg^{2+}, all with ionic radii appreciably smaller than Ca^{2+} (Table I). Again, it seems likely that smaller cations would enter and transiently occupy the D362/D367 site, but that the closed and open channel conformations bind these ions with a similar affinity, such that binding does not favor channel opening but perhaps may inhibit activation by Ca^{2+}. Previous results have, in fact, suggested that Mg^{2+} may competitively inhibit some component of activation produced by Ca^{2+} perhaps by acting at the D362/D367 site (Shi and Cui, 2001; Zhang et al., 2001).

Multiple Binding Sites and Allosteric Models of BK Channel Activation

BK channel activation at μM Ca^{2+} has been effectively described by allosteric gating models (Horrigan et al., 1999; Rothberg and Magleby, 2000; Horrigan and Aldrich, 2002; Magleby, 2003) in which a central closed–open equilibrium is independently regulated by either voltage-sensor movement or by Ca^{2+} binding. The ability of Ca^{2+} binding to favor channel activation has been proposed to involve a simple mechanical coupling mediated by a linker connecting the cytosolic structure to the pore-linking S6 helix (Niu et al., 2004). To date, the most extensive models have considered a single high affinity Ca^{2+} regulatory site per α subunit (Rothberg and Magleby, 2000; Horrigan and Aldrich, 2002; Magleby, 2003), although the consequences of including a lower affinity site on each subunit have also been considered (Shi and Cui, 2001; Zhang et al., 2001; Horrigan and Aldrich, 2002). The present results require an extension of the previous model (Horrigan and Aldrich, 2002) to include two high affinity sites along with the low affinity site. Although the apparent independence of these putative binding sites suggests that the allosteric coupling between each of the binding constants should be close to 1, further work will be required to define the allosteric interaction factors between each of the components of this complex channel.

The present results also show that mutation of a given regulatory site alters channel gating kinetics in a stereotypical fashion irrespective of whether any or all of the other sites have also been mutated. This also supports the idea that each regulatory mechanism acts independently of each other to influence distinct aspects of the overall conformational equilibria between closed and open states. For example, both high affinity sites influence transitions that contribute to Ca^{2+}-dependent increases in channel activation rate, although over different concentration ranges. In contrast, the low affinity site defined by E399 has no effects on channel activation rates, but plays a prominent role in slowing the return of channels to closed states. Together, these results support the view that there is a complex set of conformational steps in the cytosolic structure of the BK channel that are regulated in a largely independent fashion by ligation of divalent cations to three distinct sites.

We thank Lynn Lavack and Yimei Yue for preparation and injection of oocytes.

This work was supported by the National Institutes of Health grant GM066215 to C. Lingle, by the Digestive Diseases Research Core Center at Washington University (DK52574), and an AHA-Heartland affiliate fellowship to X. Zeng.

Olaf S. Andersen served as editor.

Submitted: 13 December 2004
Accepted: 21 January 2005

REFERENCES

Bao, L., C. Kaldany, E. Holmstrand, and D. Cox. 2004. Mapping the BKCa channel's "Ca^{2+} bowl": side-chains essential for Ca^{2+} sensing. *J. Gen. Physiol.* 123:475–489.

Bao, L., A. Rapin, E. Holmstrand, and D. Cox. 2002. Elimination of the BK_{Ca} channel's high affinity Ca^{2+} sensitivity. *J. Gen. Physiol.* 120:173–189.

Barrett, J.N., K.L. Magleby, and B.S. Pallotta. 1982. Properties of single calcium-activated potassium channels in cultured rat muscle. *J. Physiol.* 331:211–230.

Bian, S., I. Favre, and E. Moczydlowski. 2001. Ca^{2+}-binding activity of a COOH-terminal fragment of the *Drosophila* BK channel involved in Ca^{2+}-dependent activation. *Proc. Natl. Acad. Sci. USA.* 98:4776–4781.

Braun, A., and L. Sy. 2001. Contribution of potential EF hand motifs to the calcium-dependent gating of a mouse brain large conductance, calcium-sensitive K^+ channel. *J. Physiol.* 533:681–695.

Butler, A., S. Tsunoda, D.P. McCobb, A. Wei, and L. Salkoff. 1993. mSlo, a complex mouse gene encoding "maxi" calcium-activated potassium channels. *Science.* 261:221–224.

Cox, D.H., J. Cui, and R.W. Aldrich. 1997. Allosteric gating of a large conductance Ca-activated K^+ channel. *J. Gen. Physiol.* 110: 257–281.

Doyle, D.A., J. Morais Cabral, R.A. Pfuetzner, A. Kuo, J.M. Gulbis, S.L. Cohen, B.T. Chait, and R. MacKinnon. 1998. The structure of the potassium channel: molecular basis of K^+ conduction and selectivity. *Science.* 280:69–77.

Hamill, O.P., A. Marty, E. Neher, B. Sakmann, and F.J. Sigworth. 1981. Improved patch-clamp techniques for high-resolution current recording from cells and cell-free membrane patches. *Pflugers Arch.* 391:85–100.

Heginbotham, L., and E. Kutluay. 2004. Revisiting voltage-dependent relief of block in ion channels: a mechanism independent of punchthrough. *Biophys. J.* 86:3663–3670.

Herrington, J., C.R. Solaro, A. Neely, and C.J. Lingle. 1995. The suppression of Ca^{2+}- and voltage-dependent outward K^+ current during mAChR activation in rat adrenal chromaffin cells. *J. Physiol.* 485:297–318.

Horrigan, F., and R. Aldrich. 2002. Coupling between voltage-sensor activation, Ca^{2+} binding and channel opening in large conductance (BK) potassium channels. *J. Gen. Physiol.* 120:267–305.

Horrigan, F.T., J. Cui, and R.W. Aldrich. 1999. Allosteric voltage

gating of potassium channels I. Mslo ionic currents in the absence of Ca^{2+}. *J. Gen. Physiol.* 114:277–304.

Jiang, Y., A. Lee, J. Chen, M. Cadene, B.T. Chait, and R. MacKinnon. 2002. Crystal structure and mechanism of a calcium-gated potassium channel. *Nature.* 417:515–522.

Jiang, Y., A. Pico, M. Cadene, B.T. Chait, and R. MacKinnon. 2001. Structure of the RCK domain from the *E. coli* K^+ channel and demonstration of its presence in the human BK channel. *Neuron.* 29:593–601.

Lingle, C.J. 2002. Setting the stage for molecular dissection of the regulatory components of BK channels. *J. Gen. Physiol.* 120:261–265.

Lingle, C.J., X.-H. Zeng, J.-P. Ding, and X.-M. Xia. 2001. Inactivation of BK channels mediated by the N-terminus of the β3b auxiliary subunit involves a two-step mechanism: possible separation of binding and blockade. *J. Gen. Physiol.* 117:583–605.

Magleby, K.L. 2003. Gating mechanism of BK (Slo1) channels: so near, yet so far. *J. Gen. Physiol.* 121:81–96.

Moczydlowski, E., and R. Latorre. 1983. Gating kinetics of Ca^{2+}-activated K^+ channels from rat muscle incorporated into planar lipid bilayers. Evidence for two voltage-dependent Ca^{2+} binding reactions. *J. Gen. Physiol.* 82:511–542.

Nimigean, C.M., and C. Miller. 2002. Na^+ block and permeation in a K^+ channel of known structure. *J. Gen. Physiol.* 120:323–335.

Niu, X., X. Qian, and K.L. Magleby. 2004. Linker-gating ring complex as passive spring and Ca^{2+}-dependent machine for a voltage- and Ca^{2+}-activated potassium channel. *Neuron.* 42:745–756.

Oberhauser, A., O. Alvarez, and R. Latorre. 1988. Activation by divalent cations of a Ca^{2+}-activated K^+ channel from skeletal muscle membrane. *J. Gen. Physiol.* 92:67–86.

Pauling, L. 1960. Nature of the Chemical Bond and Structure of Molecules and Crystals. Third edition. Cornell University Press, Ithaca, NY. 644 pp.

Roosild, T.P., K.T. Le, and S. Choe. 2004. Cytoplasmic gatekeepers of K^+-channel flux: a structural perspective. *Trends Biochem. Sci.* 29:39–45.

Rothberg, B.S., and K.L. Magleby. 1999. Gating kinetics of single large-conductance Ca^{2+}-activated K^+ channels in high Ca^{2+} suggest a two-tiered allosteric gating mechanism. *J. Gen. Physiol.* 114: 93–124.

Rothberg, B.S., and K.L. Magleby. 2000. Voltage and Ca^{2+} activation of single large-conductance Ca^{2+}-activated K^+ channels described by a two-tiered allosteric gating mechanism. *J. Gen. Physiol.* 116:75–99.

Schreiber, M., and L. Salkoff. 1997. A novel calcium-sensing domain in the BK channel. *Biophys. J.* 73:1355–1363.

Schreiber, M., A. Yuan, and L. Salkoff. 1999. Transplantable sites confer calcium sensitivity to BK channels. *Nat. Neurosci.* 2:416–421.

Shi, J., and J. Cui. 2001. Intracellular Mg^{2+} enhances the function of BK-type Ca^{2+}-activated K^+ channels. *J. Gen. Physiol.* 118:589–606.

Shi, J., G. Krishnamoorthy, Y. Yang, L. Hu, N. Chaturvedi, D. Harilal, J. Qin, and J. Cui. 2002. Mechanism of magnesium activation of calcium-activated potassium channels. *Nature.* 418:876–880.

Solaro, C.R., J.P. Ding, Z.W. Li, and C.J. Lingle. 1997. The cytosolic inactivation domains of BK_i channels in rat chromaffin cells do not behave like simple, open-channel blockers. *Biophys. J.* 73: 819–830.

Sugihara, I. 1998. Activation and two modes of blockade by strontium of Ca^{2+}-activated K^+ channels in goldfish saccular hair cells. *J. Gen. Physiol.* 111:363–379.

Wei, A., C. Solaro, C. Lingle, and L. Salkoff. 1994. Calcium sensitivity of BK-type KCa channels determined by a separable domain. *Neuron.* 13:671–681.

Xia, X.-M., X.-H. Zeng, and C.J. Lingle. 2002. Multiple regulatory sites in large-conductance calcium-activated potassium channels. *Nature.* 418:880–884.

Xia, X.-M., X. Zhang, and C.J. Lingle. 2004. Ligand-dependent activation of Slo family channels is defined by interchangeable cytosolic domains. *J. Neurosci.* 24:5585–5591.

Zeng, X.H., X.M. Xia, and C.J. Lingle. 2003. Redox-sensitive extracellular gates formed by auxiliary β subunits of calcium-activated potassium channels. *Nat. Struct. Biol.* 10:448–454.

Zeng, X.-H., X.-M. Xia, and C.J. Lingle. 2001. Gating properties conferred on BK channels by the β3b auxiliary subunit in the absence of its NH_2 and COOH termini. *J. Gen. Physiol.* 117:607–627.

Zhang, X., C.R. Solaro, and C.J. Lingle. 2001. Allosteric regulation of BK channel gating by Ca^{2+} and Mg^{2+} through a nonselective, low affinity divalent cation site. *J. Gen. Physiol.* 118:607–635.